Photon pumping in a weakly-driven quantum cavity-spin system

Christina Psaroudaki[1,2] and Gil Refael[1,3]

[1] *Department of Physics and Institute for Quantum Information and Matter, California Institute of Technology, Pasadena, CA 91125, USA*
[2] *Institute for Theoretical Physics, University of Cologne, D-50937 Cologne, Germany*
[3] *Walter Burke Institute for Theoretical Physics, California Institute of Technology, Pasadena, CA 91125, USA*

(Dated: April 15, 2021)

We investigate the photon pumping effect in a topological model consisting of a periodically driven spin-1/2 coupled to a quantum cavity mode out of the adiabatic limit. In the strong-drive adiabatic limit, a quantized frequency conversion of photons is expected as the temporal analog of the Hall current. We numerically establish a novel photon pumping phenomenon in the experimentally accessible nonadiabatic driving regime for a broad region of the parameter space. The photon frequency conversion efficiency exhibits strong fluctuations and high efficiency that can reach up 80% of the quantized value for commensurate frequency combinations. We link the pumping properties to the delocalization of the corresponding Floquet states which display multifractal behavior as the result of hybridization between localized and delocalized sectors. Finally we demonstrate that the quantum coherence properties of the initial state are preserved during the frequency conversion process in both the strong and ultra-weak-drive limit.

I. INTRODUCTION

The development of efficient frequency conversion mechanisms is a process with various technological applications, relevant for quantum communications and quantum computing[1]. Photonic channels in the IR-band appear to be very attractive for the long-distance transmission of a quantum state, providing low-loss transmission[2] based on quantum-compatible storage and repeater protocols[3–5]. On the other hand, the elementary quantum processors and memories based on atoms[6–8], spins in quantum dots[9], or superconducting qubits[10], operate in different frequency regions. Thus, the realization of networks connecting disparate quantum systems[11,12] requires the development of quantum interfaces, capable of bridging the frequency gap[13–15]. The bidirectional transfer of quantum information relies on mechanisms that shift a quantum state of light from its original frequency band to a desired one, while preserving all other quantum properties[16,17].

Temporal analogs of topological models can provide a new platform for the efficient transfer of photons from one electromagnetic mode to another. In such systems, novel types of topological order are realized by subjecting a trivial quantum system to periodic driving[18–22]. In particular, driving a spin-1/2 with two elliptically polarized periodic waves of incommensurate frequencies generates the dynamical analog of a 2D topological insulator, where the Hall current corresponds to a quantized pumping of energy between the two sources[23,24]. Recently, this topological frequency conversion effect has been experimentally realized using a single-qubit IBM device[25]. Analogously, a periodically driven magnetic particle coupled to a cavity induces a quantized energy transfer from the external field to the cavity mode[26]. Such a quantized frequency conversion occurs as long as the system is in the near-adiabatic limit realized for sufficiently strong drives, when the instantaneous energy gap is large compared to the photon frequencies. Nevertheless, a rough estimation of the single-spin coupling rate to a cavity mode[27] suggests that the strong-drive requirement for a quantized energy flow is experimentally challenging.

In this work, we investigate the photon pumping effect in a topological model consisted of a periodically driven spin-1/2 coupled to a quantum cavity mode out of the adiabatic limit. The pumping properties of such a non-equilibrium system are described as the delocalization of the corresponding Floquet states in the synthetic photon-number states along the direction of the drive frequencies. To describe this phenomenon we employ a statistical analysis of the Floquet modes using the participation ratio approach, in analogy with electronic transport in the context of Anderson localization[28,29]. We thus find echos of Anderson Localization in a dynamics problem. In addition, similarly to Thouless topological charge pumping[30], the quantized energy transfer is not expected to remain robust to nonadiabatic effects. Through a nu-

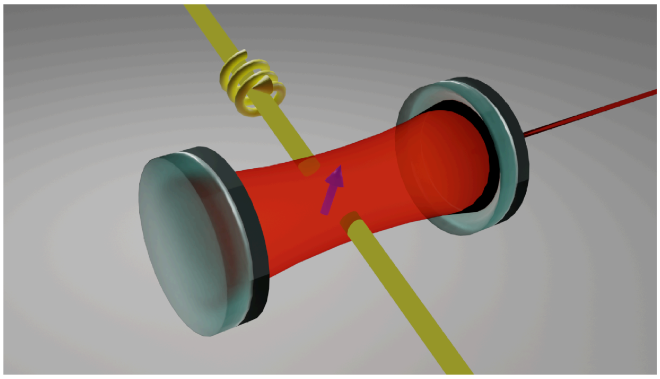

FIG. 1. Frequency conversion platform. A single spin (purple) is coupled to a cavity mode of frequency ω_1 (red) and driven by an external periodic magnetic field of frequency ω_2 (yellow).

merical estimation of the energy transfer between the two modes, we establish a novel pumping phenomenon that persists in the nonadiabatic driving regime for a broad region of the parameter space of the model.

We find that the photon pumping efficiency in the weak-driving regime exhibits strong fluctuations. For $\eta \leq \omega_i$, with η the driving amplitude and ω_i the lowest frequency, the strong fluctuations emerge due to the nonadiabatic driving conditions, before the pumping rate saturates to the quantized value for sufficiently strong drives $\eta \approx \eta_{\rm ad}$, when adiabaticity is restored. These fluctuations are stronger for rationally-related frequencies, with the conversion efficiency of the order of 80% of the quantized value for $\eta \approx 30\%\omega_1$, while in the same limit irrationally-related frequencies have a vanishing conversion efficiency. In the nonadiabatic limit and around the topological boundary, we demonstrate that a finite pumping phenomenon persists in the trivial phase, but is less effective as we move further away from the boundary. This energy pumping is characterized by a strong sensitivity to the initial phase of the drive, although we can always specify extended regions of the parameter space with efficiency that exceeds 80% of the quantized value.

A finite energy pumping signals the delocalization of the corresponding quasienergy states in the space of photon-number in the cavity. To link the pumping properties of the model to the delocalization of the Floquet states, we follow a statistical analysis of the Floquet modes, closely related to electronic transport in the context of Anderson localization[28,29], applied here to a frequency-space tight-binding model. This is achieved by calculating the inverse participation ratio and extract its scaling exponent with respect to the number of photon states. Our findings corroborate the results of the photon pumping efficiency, namely in the nonadiabatic regime commensurate frequencies have larger delocalization exponents and a finite transport of states in the nontopological regime. Perhaps the most interesting finding is that the Floquet eigenstates also display fractal behavior for any finite η as the result of hybridization between the localized and delocalized sectors, induced by the periodic drive. Note that the behavior we explore here is the complement of the non-chaotic frequenecy-locking behavior in the same system investigated in Ref. 31.

In addition, we study whether the quantum coherence properties of the initial state are preserved during the frequency conversion process, by evaluating the phase probability of the time-evolved state. During the adiabatic pumping, quantum coherence is preserved and the phase distribution is well-approximated by a Gaussian curve, although the phase undergoes a diffusion process. Surprisingly, in the ultra-weak-drive limit $\eta \ll \omega$, the pumped photon state is described by a central Gaussian peak, suggesting the existence of a state with a well defined phase. As η is increased, additional secondary peaks and phase fluctuations are generated and quantum coherence is suppressed.

The structure of the paper is as follows. In Sec. II we discuss the temporal topological models in the strong-drive regime and evaluate the quantized energy pumping for different model parameters. In Sec. III we calculate the energy flow in the weak-drive regime and identify regimes of efficient frequency conversion by exploring a broad parameter space. Such an energy flow is understood in terms of the delocalization of Floquet states, presented in Sec. IV, while the coherence properties of the pumped state are investigated in Sec. V. The experimental implications of our work are discussed in Sec. VI. Finally, our main conclusions are summarized in Sec. VII.

II. QUANTIZED ENERGY TRANSFER

The purpose of this section is to present the topological properties of an externally driven spin, coupled to a dynamical quantum mechanical cavity mode and discuss the quantized conversion of energy in the topologically nontrivial parameter regime. The quantum system is described by a Hamiltonian of the form,

$$\mathcal{H}(t) = \omega_1 \hat{n} - \eta \hat{\mathbf{B}} \cdot \hat{\boldsymbol{\sigma}} \,, \tag{1}$$

where $\hat{\boldsymbol{\sigma}} = (\sigma_x, \sigma_y, \sigma_z)$ and $\hat{\mathbf{B}} = (\hat{B}_x, \hat{B}_y, \hat{B}_z)$, with $\hat{B}_x = B_d \sin(\omega_2 t + \phi)$, $\hat{B}_y = B_0(\hat{a} - \hat{a}^\dagger)/2i$ and $\hat{B}_z = B_m - B_d \cos(\omega_2 t + \phi) - B_0(\hat{a} + \hat{a}^\dagger)/2$. Here $\hat{a}$ denotes the photon annihilation operator of the cavity mode with frequency ω_1 and amplitude B_0, $\hat{n} \equiv \hat{a}^\dagger \hat{a}$ is the photon number operator, B_m represents a static field along the z direction and B_d is the amplitude of the external periodic field of frequency ω_2 and phase ϕ. We also use $\hbar = 1$ throughout.

A rough estimation of the single-spin coupling rate to a cavity mode is given by $\eta_0 = \eta B_0 = g\mu_B \sqrt{\mu_0 \omega_c / 2\hbar V_c}$, where V_c is the cavity mode volume and ω_c the cavity frequency, further enhanced to $\eta_s = \eta_0 \sqrt{N_s}$ by utilizing an ensemble of N_s noninteracting spins[27]. For a microwave cavity mode with $\omega_c = 10$ GHz, a small $V_c = 10^{-12}$ m^3 gives $\eta_0 = 143$ Hz or $\eta = 0.32$ GHz for $N_s = 5 \times 10^{12}$ spins. The single-spin cavity strength has been experimentally measured using a X-band resonator to $\eta_0 = 0.38$ Hz and $\eta = 37.4$ MHz for $V_c = 2 \times 10^{-10}$ m^3 and $N_s = 7.8 \times 10^{14}$ [27], suggesting that the strong-drive requirement for a quantized energy flow, $\eta \gg \omega_c$, is experimentally challenging.

The model of Eq. (1) is regarded as a one dimensional semi-infinite tight-binding model, with n, the number of photons, being the lattice site. The quantized transfer of energy for incommensurate frequencies occurs in the near-adiabatic limit, when the frequencies ω_i are smaller than the instantaneous energy. Thus when $\eta \min|B_c - B_\pm| \gg \omega_i$, with $B_\pm = |B_m \pm B_d|$ and $B_c = B_0\sqrt{n}$ the effective amplitude of the electromagnetic mode in a cavity on n photons. Additionally, the system is in its topological regime when $B_c \in [B_-, B_+]$. When the spin is aligned with the instantaneous field, and under the requirements specified above, the topological effect emerges as an increase in the photon number

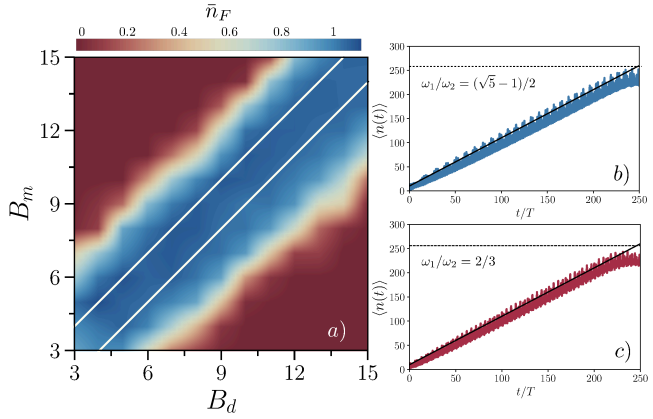

FIG. 2. a) Frequency conversion efficiency $\bar{n}_F$ in the strong-drive regime $\eta = 2$, between commensurate frequencies $\omega_1/\omega_2 = 2/3$, as a function of the amplitude of the external drive B_d and the Zeeman field B_m. We choose $N_{\rm ph} = 1$, $B_0 = 1$, $\omega_2 = 1$, and $\phi = 0$. b)-(c) Time evolution of $\langle n(t)\rangle$ for $B_m = 8 = B_d$ and b) incommensurate frequencies $\omega_1/\omega_2 = (\sqrt{5}-1)/2$ with unity efficiency $\bar{n}_F = 1$, and c) commensurate frequencies $\omega_1/\omega_2 = 2/3$ and efficiency $\bar{n}_F \approx 1$. In both cases, the number of photon in the cavity increases at the quantized rate n_Q depicted with the black solid line from the value $N_{\rm ph} = 1$ until it reaches the topological boundary $(B_m + B_d)^2/B_0 = 256$ illustrated with black dashed line at approximately time $t/T = (B_m + B_d)^2/B_0 - N_{\rm ph} = 255$.

at the quantized rate

$$n_Q = \frac{\omega_2 C}{2\pi}\,, \tag{2}$$

together with an energy transfer at the rate $dE/dt = \omega_1\omega_2 C/2\pi$ with $E = \omega_1\langle n\rangle$. We note that although the system can be chosen initially to be in its topological regime, since $B_c = B_0\sqrt{n}$ (with n here a dynamical quantity), we expect that at later times the condition $B_c \in [B_-, B_+]$ breaks down. Thus, an increase of the photon number with a quantized rate can take place as long as $n \in [B_-^2/B_0, B_+^2/B_0]$.

To address the frequency conversion in the weak-drive or commensurate frequency case, where no quantization should be expected, we numerically calculate[32] the expectation value of the photon number operator as $\langle\hat{n}(t)\rangle = \langle\Psi(t)|\hat{n}|\Psi(t)\rangle$, with $|\Psi(t)\rangle$ the time-evolved state $|\Psi(t)\rangle = U(t)|\Psi_0\rangle$ and $U(t) = \mathcal{T}\exp[-i\int_0^t \mathcal{H}(t')dt']$ the time evolution operator[32]. The Hamiltonian of Eq. (1) assumes a quantized light-matter interaction with eigenstates of the form $|n, s\rangle$, where n is the photon and s the spin index. At time $t = 0$, the system is prepared such that the spin is in its ground state $|\downarrow\rangle$, aligned with the instantaneous magnetic field, and the photon mode in a coherent state with mean number of photons $N_{\rm ph}$, $|\Psi_0\rangle = |N_{\rm ph}, \downarrow\rangle$. With this condition, $\langle\hat{n}(t)\rangle$ is an increasing function over some finite amount of time, while the initial condition $|\Psi_0\rangle = |N_{\rm ph}, \uparrow\rangle$ leads to a decreasing photon number (not considered here).

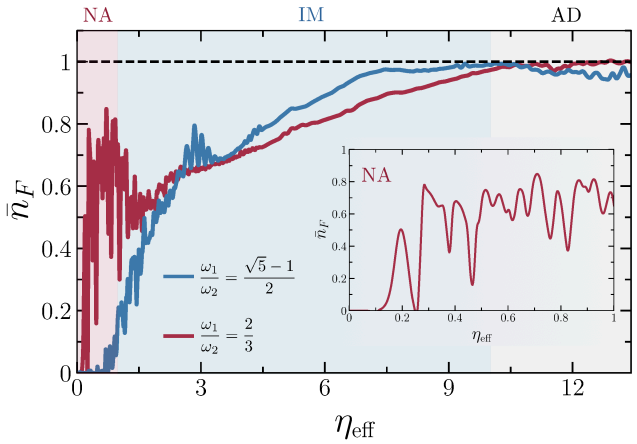

FIG. 3. Frequency conversion efficiency $\bar{n}_F$ as a function of the effective drive amplitude $\eta_{\rm eff} = \eta\sqrt{N_{\rm ph}}$, for a cavity with initially $N_{\rm ph} = 20$ photons, and a choice of $B_0 = 1$, $B_m = 8 = B_d$, $\phi = 0$, and $\omega_1/\omega_2 = (\sqrt{5}-1)/2$ (blue line) or $\omega_1/\omega_2 = 2/3$ (red line). Due to the nonadiabatic effects, the efficiency fluctuates before it converges to unity for sufficiently strong drives $\eta_{\rm ad} \approx 10$. Fluctuations are stronger for commensurate frequencies, with an efficient pumping effect $\bar{n}_F \approx 0.8$ in the deep nonadiabatic regime with $\eta_{\rm eff}$ as small as $3\% \times \eta_{\rm ad}$.

To evaluate the efficiency of the frequency conversion we use the quantized photon increase rate n_Q of Eq. (2) as a reference, and study the time-averaged photon number expectation value,

$$\bar{n}(t_{\rm max}) = \frac{2}{n_Q t_{\rm max}^2}\int_0^{t_{\rm max}} dt\ (\langle\hat{n}(t)\rangle - N_{\rm ph})\,, \tag{3}$$

where we used $\langle\hat{n}(t=0)\rangle = N_{\rm ph}$. Further, we focus on the quantity $\bar{n}_F = \bar{n}(t_{\rm top})$, where $t_{\rm top} = TB_+^2/B_0 - N_{\rm ph}$ and $T = 2\pi/\omega_2$ the period of the drive. Under this choice, we study the study the frequency conversion effect for $\langle\hat{n}(t)\rangle \in [B_-^2/B_0, B_+^2/B_0]$. Thus, for unit efficiency $\bar{n}_F = 1$, the number of photons in the cavity increases from the value $N_{\rm ph}$ up to $N_{\rm ph} + B_+^2/B_0$, at the quantized rate n_Q, a process that takes place within a $t_{\rm top}$ amount of time.

The main features of the quantized frequency conversion are depicted in Fig. 2, plotted in the strong-drive regime $\eta = 2$ and a choice of $N_{\rm ph} = 1$, $B_0 = 1$, $\omega_2 = 1$ and $\phi = 0$. Figs. 2-b) and c) suggest that in this limit, the number of photons in the cavity increases at the quantized rate n_Q, from the initial value $N_{\rm ph}$ up to the upper topological boundary B_+^2/B_0 at time $t_{\rm top}$. Choosing $B_m = 8 = B_d$, we find that incommensurate frequencies $\omega_1/\omega_2 = (\sqrt{5}-1)/2$ exhibit unit efficiency $\bar{n}_F = 1$, while commensurate frequencies $\omega_1/\omega_2 = 2/3$ can be as efficient with $\bar{n}_F \approx 1$. Finally, the colored surface of Fig. 2-a) represents the conversion efficiency $\bar{n}_F$-dependence on parameters B_m and B_d for the commensurate case $\omega_1/\omega_2 = 2/3$. White solid lines indicate the boundaries of the topological regime. Simple inspection reveals that there is a broad parameter range beyond the topological regime for which $\bar{n}_F$ reaches and even exceeds the unit

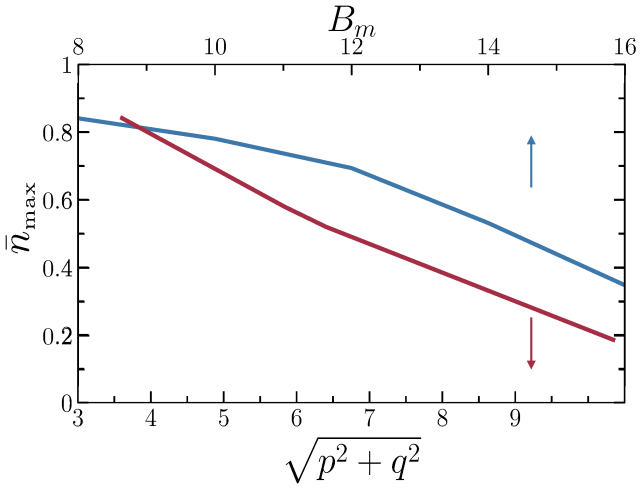

FIG. 4. Frequency conversion efficiency $\bar{n}_{\max}$ around the topological transition (blue line), and approaching irrationally-related frequencies (red line). In both cases we use $N_{\rm ph} = 20$, $B_0 = 1$ and $B_d = 8$. The blue line depicts the conversion efficiency as we vary B_m from the topological to the trivial phase for $\omega_1/\omega_2 = 2/3$ and a topological phase boundary at $B_m = 12.5$. The red line depicts the conversion efficiency for $B_m = 8$ and rationally-related frequencies of the form $\omega_1/\omega_2 = q/p$, with increasing $\sqrt{p^2+q^2}$.

efficiency.

Below we demonstrate that within this parameter region and for the experimentally accessible weak-drive limit, it is possible to transfer photons from the external mode to the cavity mode, starting from the quantum mechanical few-photon limit, with high efficiency that can reach up to $\bar{n}_F = 0.8$.

III. NONADIABATIC PUMPING

With this preparation, we turn to the main task of this paper and calculate the frequency conversion efficiency in the weak-drive regime, $\eta \leq \omega_i$. In analogy with the quantization of the charge transport upon a cyclic adiabatic driving of a band insulating system, known as Thouless topological pumping[30], the quantized energy transfer is not expected to remain robust in the face of nonadiabatic effects[33]. In the adiabatic limit discussed in Sec. II-B, the non-quantized pumping power for commensurate frequencies is understood in terms of a partial sampling of the Berry curvature, contrary to the incommensurate case with a robust quantized pumping proportional to $C = 1$. Thus, for an efficient pumping beyond the topological regime, it appears promising to tune the photon frequencies to a rational ratio. At time $t = 0$, the system is in the state $|\Psi_0 = |N_{\rm ph}, \downarrow\rangle$.

In Fig. 3 we plot the frequency conversion efficiency $\bar{n}_F$ as a function of the effective drive amplitude $\eta_{\rm eff} = \eta\sqrt{N_{\rm ph}}$, for a cavity with initially $N_{\rm ph} = 20$ photons in the topological regime with $B_0 = 1$ and $B_m = 8 = B_d$. We examine both rational $\omega_1/\omega_2 = 2/3$ (red line) and irrational $\omega_1/\omega_2 = (\sqrt{5}-1)/2$ frequency combinations in a broad region of the driving amplitude including the nonadiabatic (NA) $\eta_{\rm eff} \leq \omega_i$ (red shaded area), the intermediate (IM) $\omega_i \lessapprox \eta_{\rm eff} \leq \eta_{\rm ad}$ (blue shaded area), and the adiabatic regime (AD) (gray shaded are) for $\eta_{\rm eff} \geq \eta_{\rm ad}$. Fig. 3 allows for two major observations. First, for both frequency combinations, due to the nonadiabatic effects, $\bar{n}_F$ strongly fluctuates before it converges to unity for sufficiently strong drives $\eta_{\rm ad} \approx 10$. In addition, in the nonadiabatic regime depicted in detail in the inset of Fig. 3, fluctuations are stronger for rational frequencies, with efficient pumping effects of the order of $\bar{n}_F \approx 0.8$ at $\eta_{\rm eff}$ that could be as small as $30\%\omega_1$. For intermediate amplitudes $2 \lessapprox \eta_{\rm eff} \lessapprox 6$, thus for $\eta_{\rm eff} \approx 20 - 60\% \times \eta_{\rm ad}$, there is still a finite photon pumping $0.5 \lessapprox \bar{n}_F \lessapprox 0.8$, a behavior that is independent of the frequency combination. To justify the choice of the field amplitude $B_m = 8 = B_d$, we note for the parameters summarized in Fig. 2-3, the frequency conversion effect takes place within a sufficiently long time interval $t_{\rm top} = 1071$, during which the cavity photon number is increased by $\Delta n = \langle \hat{n}(t_{\rm top})\rangle - \langle \hat{n}(0)\rangle = 256$ photons. In physical units, $t_{\rm top} = 1$ μs for $\omega_1 = 1$ GHz, while both B_m and B_d are in the mT regime.

In the nonadiabatic regime $\eta_{\rm eff} \leq \omega_i$, irrational frequencies display vanishing efficiency $\bar{n}_F = 0$. Such a striking contrast of the nonadiabatic pumping between commensurate and incommensurate frequencies is understood as follows. The energy pumping in the adiabatic regime is generated by engineering synthetic dimen-

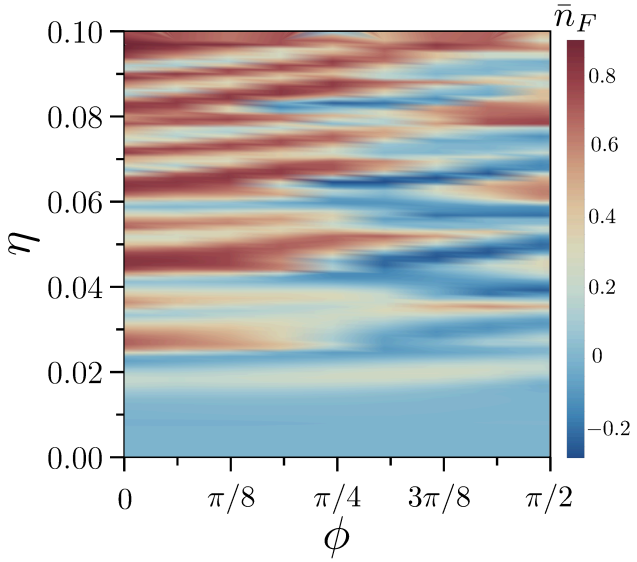

FIG. 5. The colored surface represents the conversion efficiency $\bar{n}_F$ as a function of the initial phase of the external periodic drive ϕ and the drive amplitude η, with $B_0 = 1$, $\omega_1/\omega_2 = 2/3$, $N_{\rm ph} = 100$ and $B_m = 20 = B_d$. We observe that $\bar{n}_F$ is highly sensitive with respect to both η and ϕ.

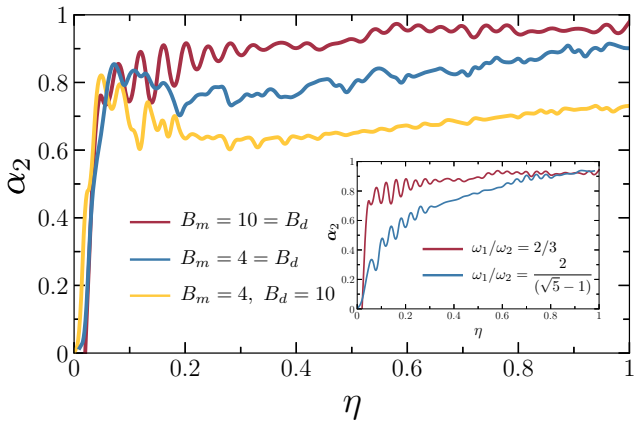

FIG. 6. Inverse participation ratio exponent α_2 as a function of the driving amplitude η for $\omega_1/\omega_2 = 2/3$ and $B_0 = 1$. We use three different parameter combinations, two in the topological regime $B_m = 10 = B_d$ (red line) and $B_m = 4 = B_d$ (blue line), and one in the trivial regime $B_m = 4$, $B_d = 10$. The inset depicts $\alpha_2(\eta)$ for $B_0 = 1$, $B_m = 10 = B_d$, and $\omega_1/\omega_2 = 2/3$ (red line) or $\omega_1/\omega_2 = 2/(\sqrt{5}-1)$ (blue line).

sions, where each lattice dimension equals the number of irrationally-related drive frequencies. When the two frequencies have a rational ratio, $\omega_1/\omega_2 = q/p$ with p, q coprime integers, the two-dimensional lattice is compactified into a cylinder of circumference $\sqrt{p^2+q^2}$[23]. Thus, in the limit of $p, q \gg 1$, one expects the pumping to be insensitive to the details of the frequency ratio and obtain its universal value which derives from the underlying topology. In turn, the topological effect cannot apply at weak drive. This is supported by the results summarized in Fig. 4 (red line), where we plot $\bar{n}_{\max}$ in the nonadiabatic regime for $N_{\rm ph} = 20$, $B_0 = 1$, $B_m = B_d = 8$, and various frequency combinations. Here $\bar{n}_{\max}$ is defined as the maximum value of $\bar{n}_F$ in the nonadiabatic regime, $\bar{n}_{\max} = \max\{\bar{n}_F(\eta_{\rm eff}) : \eta_{\rm eff} \in [0,1]\}$. It becomes apparent that as p, q increase, the nonadiabatic pumping effect vanishes. The full fluctuating behavior of $\bar{n}_F(\eta_{\rm eff})$ is presented in Fig. 12.

Let us now focus on the conversion efficiency around the topological transition, as illustrated in Fig. 4 (blue line). We present $\bar{n}_{\max}$ as a function of B_m for $B_0 = 1$, $B_d = 8$, $\omega_1/\omega_2 = 2/3$, and a topological phase boundary at $B_m = 12.47$. The overall picture suggested is that a finite $\bar{n}_F$ persists in the nontopological regime but with intensity that vanishes as we go further away from the topological boundary. The full fluctuating behavior of $\bar{n}_F(\eta_{\rm eff})$ is presented in Fig. 13.

To complete the description we must also examine the sensitivity of $\bar{n}_F$ to the initial phase of the external periodic drive ϕ, due to dephasing of the time evolved state $|\Psi(t)\rangle$. The main features are depicted in Fig. 5, where we plot $\bar{n}_F$ as a function of both η and ϕ and a choice of $B_0 = 1$, $\omega_1/\omega_2 = 2/3$, $N_{\rm ph} = 100$ and $B_m = 20 = B_d$. We observe that although $\bar{n}_F$ is highly sensitive with respect to both η and ϕ, we can specify extended regions of the parameter space with efficient pumping $\bar{n}_F \geq 0.8$. This sensitivity on ϕ is a remnant of an analogous ϕ-dependence of $\bar{n}_F$ in the adiabatic regime, where the pumping effect is proportional to the integral of the Berry curvature along a path selected by ϕ, further enhanced here by the nonadiabatic driving conditions. The sensitivity of $\bar{n}_F$ on the initial conditions motivates studies on the statistical behavior of the pumping effect for an ensemble of random Hamiltonians. The distribution of the energy pumping efficiency along with the Floquet level statistics is explored in a subsequent publication 34.

IV. FLOQUET LOCALIZATION

A finite energy pumping in a frequency-space tight-binding model signals the delocalization of the corresponding quasienergy states along the direction of the drive frequencies, that now play the role of an effective electric field. In this section we link the pumping properties of the quantum cavity-spin model to the delocalization properties of its Floquet modes. In the case of a simple periodic drive with frequency ω_2, the time evolution of an arbitrary initial state has the form[35]

$$|\Psi(t)\rangle = \sum_j c_j e^{-i\varepsilon_j t}|u_j(t)\rangle\,, \tag{4}$$

where ε_j are the quasienergies and c_j are time-independent coefficients. The Floquet states $|u_j(t)\rangle$ diagonalize the single-period time evolution operator $U(T) = \mathcal{T}\exp[-i\int_0^T \mathcal{H}(t')dt']$, where $T = 2\pi/\omega_2$ is the period of the drive.

Based on an expansion of the zero time Floquet states in the photon basis $|u_j(0)\rangle = \sum_n b_j^n|n\rangle$, the generalized

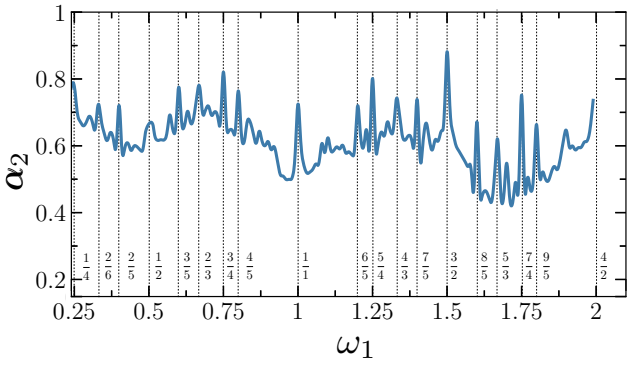

FIG. 7. Inverse participation ratio exponent α_2 for $B_0 = 1$, $B_m = 10 = B_d$, $\eta = 0.16$, $\omega_2 = 1$ and various frequency combinations ω_1. We note that α_2 is maximized for commensurate frequencies.

inverse participation ratio (IPR) is defined as[36]

$$\mathcal{R}_q = \frac{1}{N}\sum_{j,n=0}^{N-1} |b_j^n|^{2q} = \frac{1}{N^{\alpha_q}}\,, \tag{5}$$

where N is both the number of the Floquet modes and the number of photons in the cavity, while for convenience we first focus on $\mathcal{R}_2$. If a Floquet state is delocalized among many photon states, then each of them contributes $b_j^n \approx 1/\sqrt{N}$ and $\mathcal{R}_2 \approx 1/N$ for $N \gg 1$ ($\alpha_2 = 1$). In the opposite limit, a localized Floquet state in the photon lattice will give $\mathcal{R}_2 = 1$ ($\alpha_2 = 0$). For a given set of parameters and driving amplitude η, we calculate $\mathcal{R}_2$ for $N \in [10, 200]$ and extract the exponent α_2 by a numerical fit.

In Fig. 6 we plot the exponent α_2 for the model (1) as a function of the driving amplitude η and examine its behavior as the system transitions from the topological to the trivial regime. In the topological class, Floquet states are delocalized for any finite η with α_2 exhibiting strong fluctuations in the $0 \leq \eta \leq 0.2$ regime around $\alpha_2 \approx 0.8$, before it asymptotically approaches $\alpha \to 1$ for larger η. In the trivial class and for large η, $\alpha_2 \to \alpha_{\rm as}$ with $\alpha_{\rm as} < 1$, indicating a hybridization between the localized and delocalized sectors. The inset depicts the delocalization of Floquet states in the topological regime $B_0 = 1$ and $B_m = 10 = B_d$ for commensurate $\omega_1/\omega_2 = 2/3$ (red line) and incommensurate $\omega_1/\omega_2 = 2/(\sqrt{5}-1)$ (blue line) frequency combinations. As expected, in the nonadiabatic regime commensurate frequencies have larger delocalization exponents, that is translated into large photon pumping in the cavity. This is further supported by the results summarized in Fig. 7 for $B_0 = 1$, $B_m = 10 = B_d$, $\eta = 0.16$ and various frequency combinations ω_1. We note that α_2 is significantly enhanced for commensurate frequency combinations, corroborating the results of Sec. III.

Perhaps the most interesting finding is that in all cases the scaling exponent of $\mathcal{R}_2$ reflects a hybridization between the localized and delocalized sectors, that is a sign of Floquet multifractality. The presence of multifractal states is associated with the critical spectral statistics of a system exactly on the metal- insulator transition point[37] or the Anderson transition point[38,39]. To analyze the multifractal behavior of the Floquet eigenstates of the driven quantum-cavity system, we examine the generalized IPR of Eq. (5) as a function of the fractal dimension q. For localized states it holds $\alpha_q = 0$, for delocalized $\alpha_q = q - 1$, and any other combination signals multifractionality. The overall picture suggested by Fig. 8, where we plot α_q for three values of the drive $\eta = 0.01, 0.1, 0.5$, is that multifractality of the Floquet states is present for any $\eta > 0$ and Floquet states become increasingly delocalized with increasing η. This surprising result motivates further studies on the criticality of the Floquet eigenstate statistics[40] but is beyond the scope of the present paper and we leave it for the future.

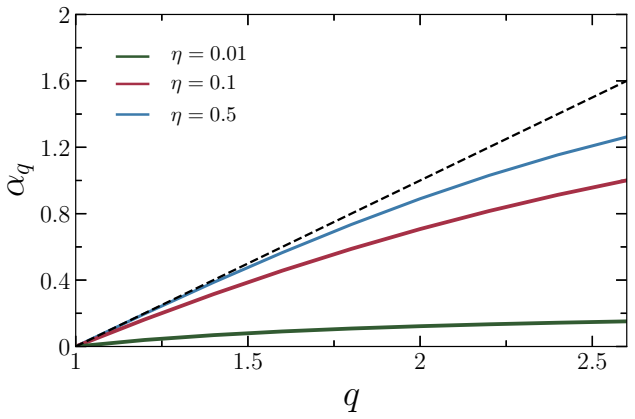

FIG. 8. Inverse participation ratio exponent α_q as a function of the fractal dimension q for $B_0 = 1$, $B_m = 10 = B_d$, $\omega_1/\omega_2 = 2/3$ and three driving amplitudes $\eta = 0.01, 0.1$, and 0.5. The black dashed line denotes the expected $\alpha = q - 1$ behavior for delocalized states.

V. QUANTUM COHERENCE

In this section we study the coherent properties of the pumped time-evolved photon state $|\Psi(t)\rangle$ to examine whether the phase coherence of the initial state is preserved during the frequency conversion process, a necessary condition for a quantum information transfer[12]. In the context of quantum optics, a number of probability distributions can be employed to investigate the properties of quantum states. Here we focus on the Pegg-Barnett phase probability distribution based on a construction of a Hermitian phase operator to study whether outgoing states have a well defined phase[41]. We introduce a complete set of orthonormal phase states[41]

$$|\theta_m\rangle = \frac{1}{N}\sum_{n,s} e^{in\theta_m}|n,s\rangle\,, \tag{6}$$

where $\theta_m = 2\pi m/N$, $m = 0, \cdots, N-1$, $|n,s\rangle$ are eigenstates of the coupled photon-spin system and N is the total number of photon states. The phase probability distribution $P(\theta) = |\langle\theta|\Psi\rangle|^2$ contains important information on the phase properties of a general state $|\Psi\rangle$. Here we initially prepare the system at a coherent photon state $N_{\rm ph}$ and the spin aligned with the magnetic field, $|\Psi_0\rangle = |N_{\rm ph},\downarrow\rangle$ and let it evolve under the driven spin-cavity Hamiltonian $\mathcal{H}(t)$ of Eq. (1).

The quantum coherence properties of the pumped photon state $|\Psi(t)\rangle$ in the adiabatic limit are summarized in Fig. 9, for parameters in the topological phase $B_0 = 1$, $B_m = 8 = B_d$, $\omega_2 = 1$, commensurate frequencies $\omega_1/\omega_2 = 2/3$, and strong drive $\eta = 10/\sqrt{N_{\rm ph}}$. Panel a) depicts the time evolution of the Pegg-Barnett phase distribution $P(\theta)$ for $N_{\rm ph} = 20$. As expected quantum coherence is maintained and $P(\theta)$ is described by a Gaussian peak at all times [see Fig. 9-b) and c)], although the standard deviation σ_θ of the distribution increases

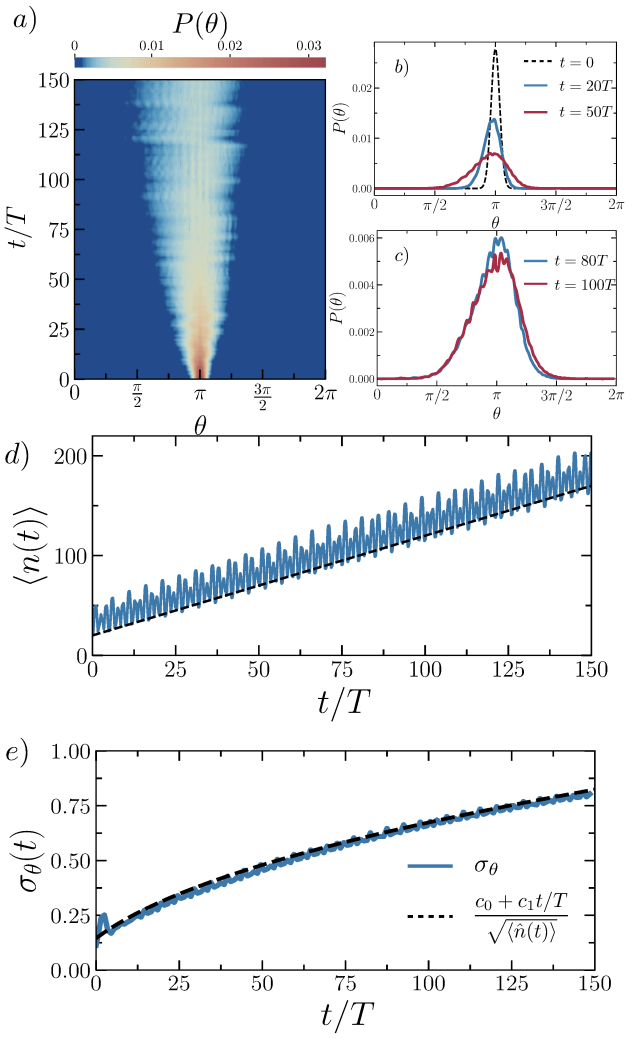

FIG. 9. Quantum coherence properties of the pumped photon state in the adiabatic limit $\eta = 10/\sqrt{N_{\rm ph}}$. a) Time evolution of the phase distribution $P(\theta)$ for $B_0 = 1$, $B_m = 8 = B_d$ (topological phase), $\omega_1/\omega_2 = 2/3$, and $N_{\rm ph} = 20$. $P(\theta)$ follows a Gaussian distribution with a standard deviation σ_θ an increasing function over time. b), c) Snapshots of the phase distribution $P(\theta)$ at several time incidents between $t = 0$ and $t = 100$. d) Time evolution of $\langle n(t)\rangle$ with $\bar{n}_F = 1$. e) Time evolution of σ_θ, well approximated by $\sigma_\theta(t) = (c_0 + c_1 t/T)/\sqrt{\langle \hat{n}(t)\rangle}$, with $c_0 = 0.65$ and $c_1 = 0.068$.

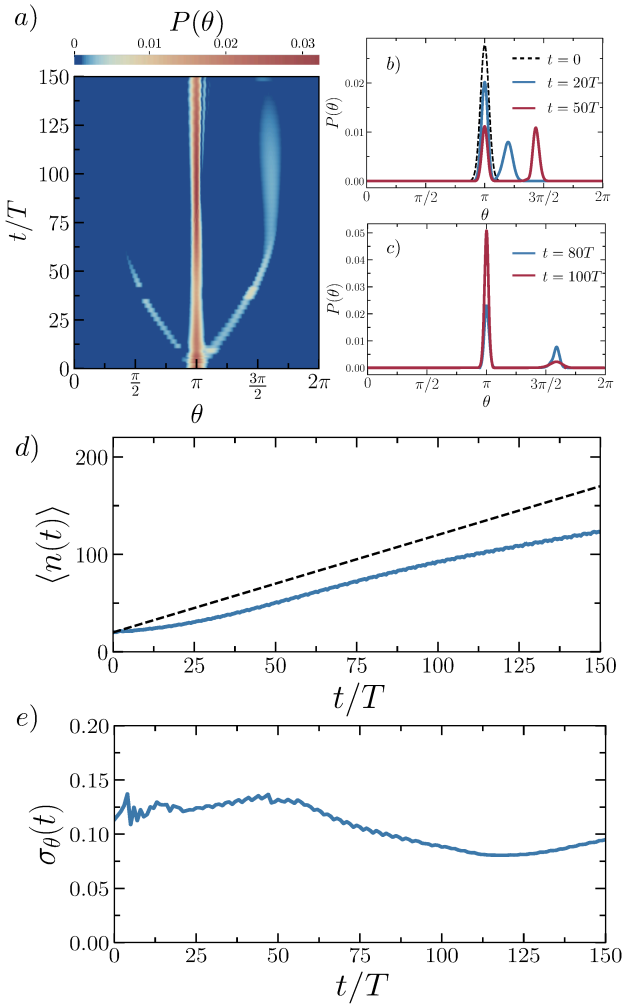

FIG. 10. Quantum coherence properties of the pumped photon state in the nonadiabatic limit $\eta = 0.3/\sqrt{N_{\rm ph}}$. a) Time evolution of the phase distribution $P(\theta)$ for $B_0 = 1$, $B_m = 8 = B_d$ (topological phase), $\omega_1/\omega_2 = 2/3$, and $N_{\rm ph} = 20$. b), c) Snapshots of the phase distribution $P(\theta)$ at several time incidents between $t = 0$ and $t = 100$. d) Time evolution of $\langle n(t)\rangle$ with $\bar{n}_F \approx 0.8$. e) Time evolution of σ_θ of the central Gaussiann peak.

over time [see Fig. 9-e)]. The photon number $\langle n(t)\rangle$ increases over time at the quantized rate n_Q [see Fig. 9-d)]. The standard deviation σ_θ is well approximated by $\sigma_\theta(t) = (c_0 + c_1 t/T)/\sqrt{\langle n(t)\rangle}$ with $c_0 = 0.65$, $c_1 = 0.068$, and $T = 2\pi/\omega_2$.

The broadening of the Gaussian curve suggests that the phase of the pumped state undergoes a diffusion process, evident in the time evolution of both the mean amplitude $\langle \hat{a}(t)\rangle$ and $\langle e^{i\hat{\Phi}_\theta}(t)\rangle$. Here $\hat{a}$ is the photon annihilation operator and $\hat{\Phi}_\theta = \sum_m \theta_m |\theta_m\rangle\langle\theta_m|$ is the phase operator. In Fig. 11 we present $\langle \hat{a}(t)\rangle/\langle \hat{n}(t)\rangle$ (upper panel) and extract the rate of amplitude decay as $\Gamma_n = 1.7 \times 10^{-3}$, a direct measure of the phase diffusion rate[42]. The lower panel depicts $|\langle e^{i\hat{\Phi}_\theta}(t)\rangle| = e^{-\frac{1}{2}\sigma_\theta^2(t)} \approx e^{-\Gamma_\theta t}$ with $\Gamma_\theta = c_1^2/2T = 3.66 \times 10^{-4}$. Thus, the outgoing pumped state is described by a diffusion coefficient $\Gamma_\theta \approx 3.66 \times 10^{-4} \times \omega_1$, a quantity that is equivalent to a single-mode laser linewidth. Typically, narrow-band sources are preferable for quantum information applications as they provide access to atomic transitions.

The quantum coherence properties of the pumped photon state $|\Psi(t)\rangle$ in the nonadiabatic limit are summarized in Fig. 10, for parameters in the topological phase $B_0 = 1$, $B_m = 8 = B_d$, commensurate frequencies $\omega_1/\omega_2 = 2/3$, and ultra-weak drive $\eta = 0.3/\sqrt{N_{\rm ph}}$. Panel a) depicts the time evolution of the Pegg-Barnett phase

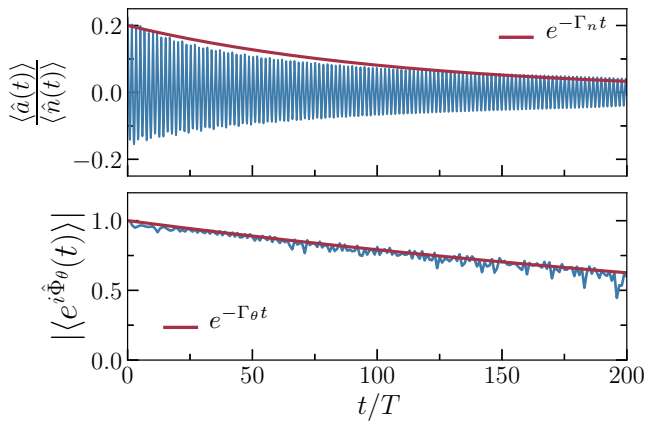

FIG. 11. Time evolution of the mean amplitude $\langle \hat{a}(t)\rangle/\langle \hat{n}(t)\rangle$ (upper panel) and $\langle e^{i\hat{\Phi}_\theta}(t)\rangle$ (lower panel) for $\eta = 10/\sqrt{N_{\rm ph}}$, $B_0 = 1$, $B_m = 8 = B_d$, $\omega_1/\omega_2 = 2/3$, and $N_{\rm ph} = 20$. The rate of the amplitude decay is $\Gamma_n = 0.011$ for the former and $\Gamma_\theta = 0.0023$ for the later. We note that on top of the exponential behavior, $\langle \hat{a}(t)\rangle/\langle \hat{n}(t)\rangle$ oscillates at a frequency $\omega_1 = 2/3$.

distribution $P(\theta)$ for $N_{\rm ph} = 20$. $P(\theta)$ is still described by a central Gaussian peak [see Fig. 9 b) and c)], although additional peaks develop due to the nonadiabatic driving conditions. Thus, the standard deviation σ_θ, plotted in Fig. 10-e), increases/decreases over time due to the appearance/disappearance of secondary peaks. For all cases plotted, the photon number in the cavity increases over time with frequency conversion efficiency $\bar{n}_F \approx 0.8$. As we further increase η additional phase fluctuations are generated and phase coherence is suppressed. A summary of this behavior is depicted in Fig. 14 of the Appendix, where we also illustrate how phase coherence is restored as the system approaches the strong-drive adiabatic limit.

In summary, the frequency conversion in the adiabatic limit preserves the quantum coherence properties of the initial state, although the state is characterized by a diffusion coefficient. For nonadiabatic driving conditions and ultra-low drive, $P(\theta)$ is still described by a central Gaussian peak, suggesting that the pumped quantum state has a well defined phase. As we further increase the driving amplitude, additional secondary peaks and phase fluctuations are generated and quantum coherence is suppressed.

VI. EXPERIMENTAL IMPLICATIONS

Here we discuss whether the nonadiabatic frequency conversion discussed in the previous section is experimentally feasible. To give an estimate in physical units under the choice of parameters summarized in Fig. 3, thus for $B_0 = 1$ and $B_d = 8 = B_m$, we first note that the adiabatic requirement holds as long as $\eta \geq \hbar\omega_1\eta_{\rm ad}/\sqrt{N_{\rm ph}} \approx 10\hbar\omega_1/\sqrt{N_{\rm ph}}$. Therefore, in the few-photon limit, starting with a state of $N_{\rm ph} = 20$ *coherent* photons, the adiabatic requirement is met for a spin-photon coupling of the order of $\eta/h\omega_1 = 0.18$ at $B_d = B_m = 100$ mT, and grows to $\eta/h\omega_1 = 0.8$ in the fully quantum limit with $N_{\rm ph} = 1$ and $B_d = B_m = 450$ mT. In the opposite many-photons limit, starting with a cavity of $N_{\rm ph} = 200$ photons, the adiabatic limit corresponds to $\eta/h\omega_1 = 0.06$ at 32 mT, and for $N_{\rm ph} = 400$ we find $\eta/h\omega_1 = 0.04$ at 23 mT. On the contrary, a nonadiabatic pumping is possible for even smaller values of the spin-photon coupling of approximately $\eta = 0.3\hbar\omega_1/\sqrt{N_{\rm ph}}$. This translates to $\eta/h\omega_1 = 5.3\times10^{-3}$ for $N_{\rm ph} = 20$ at 3 mT, and $\eta/h\omega_1 = 2.4\times10^{-2}$ for $N_{\rm ph} = 1$ at 14 mT.

The direct interaction of a single spin with the cavity magnetic field is exceedingly small, with $\eta_0/h\omega_1 = 10^{-9}$. A generalization is to consider of an ensemble of N_s identical two-level systems resonantly interacting with a single electromagnetic field, a model analyzed by Tavis and Cummings[43]. In the scope of this model, the collective spin-photon coupling is $\eta = \sqrt{N_s}\eta_0$, where η_0 is the coupling strength of each individual spin, a scaling that has been experimentally verified, while a similar $\sqrt{N_s}$ behavior prevails also for the magnon-photon coupling in magnetically interacting systems[44–48]. The coupling of large electron spin ensembles to microwave cavity photons has been experimentally found to be of the order of $\eta/h\omega_1 = 5\times10^{-4}$ ($\omega_1 = 9.7$ GHz) for a large ensemble of $N_s = 10^{16}$ spins in a 3D microwave cavity[27], and of the order of $\eta/h\omega_1 = 4\times10^{-3}$ for $N_s = 10^{12}$ spins in a superconducting cavity[49,50] ($\omega_1 = 2.87$ GHz at 40 mK).

Several approaches have been explored in order to enhance the spin-photon coupling. Recently, it has been demonstrated that by reducing the cavity effective volume at superconducting nanoconstrictions, the microwave magnetic field is enhanced and results strong spin-photon couplings of the order of $\eta/h\omega = 1.4\times10^{-3}$ for $N_s = 10^8$ spins in a microwave cavity with an average of 5×10^5 thermal photons[51] ($\omega_1 = 1.4$ GHz at 44 mK). A different approach is to consider a number of exchange-coupled spins, where the coupling strength is reported to be at least one order of magnitude larger as compared to noninteracting spins, *i.e.* $\eta/h\omega_1 = 7.6\times10^{-2}$ [44] ($\omega_1 = 5.6$ GHz at 50 mK). In these systems, microwave cavity photons interact coherently with the collective spin excitations in ferromagnetic crystals[48], such as the ferromagnetic insulator yttrium iron garnet (YIG). A strong coupling is achieved when the cavity and the magnetostatic mode are on resonance, leading to $\eta/h\omega_1 \approx 3\times10^{-3}$ [45] ($\omega_1 = 10.6$ GHz at 10 mK). The resonance condition justifies the single photon mode assumption in the model of Eq. 1, as higher-energy modes are off-resonant and can be neglected. This is further supported by the results of Ref. 26 in a classical multi-mode cavity, where the authors demonstrated that the energies of higher-energy modes, effectively suppressed by tuning their dissipation rates, decay fast to zero. In view of the increasing interest on the coherent interaction between magnons and

microwave or optical photons, we believe our work could serve as a basis for studies on photon frequency conversion in a system of N_s *interacting* spins, also motivated by recent results on the enhancement of frequency conversion in a system of two interacting spins[52].

Nevertheless, in the above studies the spin-phonon coupling has been explored away from the quantum single-spin to single-photon limit. A promising platform for the realization of the Tavis-Cummings model is the use of two-state atoms coupled to a resonant cavity mode with a large reported single-qubit to single-photon coupling of the order of $\eta_0/h\omega_1 = 1.3 \times 10^{-2}$ [53]$\omega_1 = 6.7$ GHz at 20 mK). The coupling of single electron spins in silicon quantum dots to single microwave photons has been reported to be of the order of $\eta_0/h\omega_1 = 2 - 7 \times 10^{-3}$, with an average thermal photon number in the resonator well below 1[54–56] ($\omega_1 = 7.7$ GHz at $10 - 30$ mK). Finally, at room temperature, the magnon to microwave photon coupling is of the order of $\eta/h\omega_1 = 1.4 - 3.3 \times 10^{-3}$ [46,47] ($\omega_1 = 7.9$ GHz), while the spin-photon coupling in a molecular crystal is $\eta/h\omega_1 = 1.2 \times 10^{-3}$ [57] ($\omega_1 = 1.45$ GHz). From the above considerations it becomes apparent that the predicted frequency conversion effect in the nonadiabatic limit is experimentally feasible using a large ensemble of spins and is within experimental reach for the quantum few-photon limit.

VII. DISCUSSION

In this work, we consider the transfer of energy in a periodically driven spin-1/2 coupled to a quantum cavity mode out of the adiabatic limit. We establish a novel pumping phenomenon that persists in the weak-drive regime and examine its efficiency for a broad range of the parameter space. We demonstrate that the frequency conversion efficiency exhibits strong fluctuations due to the nonadiabatic effects before it saturates to unity for sufficiently strong drives, $\eta_{\rm ad} \approx 10\omega_i$. It is more efficient for rationally-related frequencies and can reach up to 80% of the quantized value for $\eta = 0.3\omega_i$. Emphasis is put on the magnitude of the pumping effect in the nontopological phase of the model. A finite frequency conversion efficiency persists in the trivial phase, but is less effective as we move further away from the topological boundary.

A finite-energy pumping signals the delocalization of the corresponding Floquet states, which are found to display a multifractal behavior, due to the hybridization between localized and delocalized sectors. The presence of multifractal states, associated with critical spectral statistics, motivates future studies on the criticality of the Floquet eigenstate statistics. Finally, we show that in the adiabatic limit, during the frequency conversion process, the quantum coherent properties of the initial state are preserved, but the phase undergoes a diffusion process. For ultra-low drive, the pumped quantum state has still a well defined phase but as we further increase the driving amplitude, additional secondary peaks and

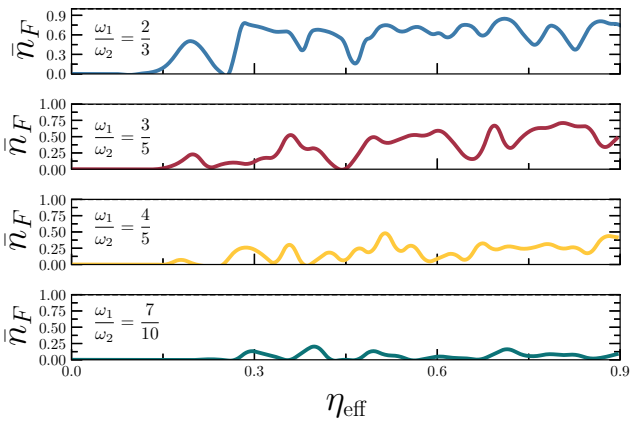

FIG. 12. Frequency conversion efficiency $\bar{n}_F$ as a function of the effective drive amplitude $\eta_{\rm eff} = \eta\sqrt{N_{\rm ph}}$, for a cavity with initially $N_{\rm ph} = 20$ photons in the topological class $B_0 = 1$, and $B_m = 8 = B_d$. Four different commensurate frequency combinations are presented of the form $\omega_1/\omega_2 = q/p$, with increasing $\sqrt{p^2+q^2}$. When $q, p \gg 1$, the nonadiabatic photon pumping vanishes.

phase fluctuations are generated and quantum coherence is suppressed.

Experimental systems are subject to dissipation mechanisms that need to be incorporated for the construction of a realistic model (although we don't expect a qualitative change of our results). In the adiabatic driving limit and within a Markov-Lindblad framework, the inclusion of external noise and dissipation stabilizes the conversion effect as the system approaches a steady state with a quantized number of emitted photons per driving period[26]. In the nonadiabatic limit, it was recently demonstrated that the introduction of a non-Hermitian tailored time-periodic dissipation restores the topological transport quantization of Thouless pumps in plasmonic waveguide arrays, emphasizing the uniqueness of Floquet topological systems[58].

ACKNOWLEDGMENTS

We are grateful to Ivar Martin and Frederik Nathan for useful discussions. C.P. has received funding from the European Union's Horizon 2020 research and innovation program under the Marie Sklodowska-Curie grant agreement No 839004. We are also grateful to the U.S. Department of Energy, Office of Science, Basic Energy Sciences under Award de-sc0019166. GR is also grateful to the NSF DMR grant number 1839271. NSF and DOE supported GR's time commitment to the project in equal shares. NSF provided partial support to C.P. This work was performed in part at Aspen Center for Physics, which is supported by National Science Foundation grant PHY-1607611. G.R. is also grateful for support from the Simons Foundation and the Packard Foundation.

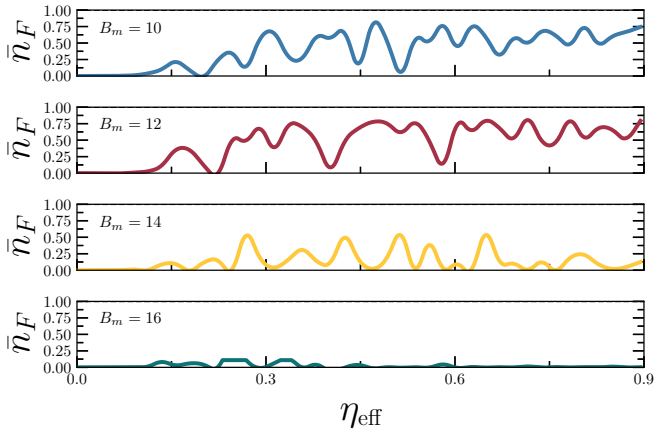

FIG. 13. Frequency conversion efficiency $\bar{n}_F$ as a function of the effective drive amplitude $\eta_{\rm eff} = \eta\sqrt{N_{\rm ph}}$, for a cavity with initially $N_{\rm ph} = 20$ photons, $B_0 = 1$, $B_d = 8$, and $\omega_1/\omega_2 = 2/3$. Four different Zeeman fields are presented, two in the topological phase, $B_m = 10, 12$ and two in the trivial phase $B_m = 14, 16$. The topological phase boundary is at $B_m = 12.47$.

Appendix A: Appendix

In this Appendix we provide further details on the frequency conversion effect. In Fig. 12 we plot the dependence of the frequency conversion efficiency $\bar{n}_F$ on $\eta_{\rm eff}$, for a cavity with initially $N_{\rm ph} = 20$ photons in the topological class $B_0 = 1$, $B_m = 8 = B_d$, and four different commensurate frequency combinations of the form $\omega_1/\omega_2 = q/p$. We note that as $q, p \gg 1$, the nonadiabatic pumping effect vanishes, and the overall behavior resembles the one for irrationally-related frequencies.

Moreover, we are interested in exploring whether the pumping effects persists for parameters outside the topological regime. We therefore plot $\bar{n}_F$ as a function of $\eta_{\rm eff}$ for a cavity with initially $N_{\rm ph} = 20$ photons, $B_0 = 1$, $B_d = 8$ and $\omega_1/\omega_2 = 2/3$ and four different values of the Zeeman field amplitude. The topological phase boundary is at $B_m = 12.5$. Although the pumping effects persists in the trivial phase of the model, the intensity diminishes as we go further away from the boundary.

Finally, for completeness we present the phase distribution $P(\theta)$ calculated in Sec. V for parameters ranging between the ultra-weak-drive up to the strong-drive limit. In Fig. 14 we present $P(\theta)$ for seven values of η, $B_0 = 1$, $B_m = 8$, $B_d = 8$, $N_{\rm ph} = 20$, and $\omega_1/\omega_2 = 2/3$. Phase coherence is preserved in the ultra-weak limit $\eta \ll \omega_i$, and $P(\theta)$ is described by a central Gaussian peak. As η is increased, additional secondary peaks and phase fluctuations are generated and the pumped states is no longer characterized by a well defined phase. Phase coherence is restored in the strong-drive adiabatic limit, where $P(\theta)$ is a Gaussian curve at all times.

[1] N. Lauk, N. Sinclair, S. Barzanjeh, J. P. Covey, M. Saffman, M. Spiropulu, and C. Simon, Quantum Science and Technology **5**, 020501 (2020).
[2] J. L. O'Brien, A. Furusawa, and J. Vučković, Nature Photonics **3**, 687 (2009).
[3] H.-J. Briegel, W. Dür, J. I. Cirac, and P. Zoller, Phys. Rev. Lett. **81**, 5932 (1998).
[4] T. Chanelière, D. N. Matsukevich, S. D. Jenkins, T. A. B. Kennedy, M. S. Chapman, and A. Kuzmich, Phys. Rev. Lett. **96**, 093604 (2006).
[5] L.-M. Duan, M. D. Lukin, J. I. Cirac, and P. Zoller, Nature **414**, 413 (2001).
[6] A. D. Boozer, A. Boca, R. Miller, T. E. Northup, and H. J. Kimble, Phys. Rev. Lett. **98**, 193601 (2007).
[7] T. Chanelière, D. N. Matsukevich, S. D. Jenkins, S.-Y. Lan, T. A. B. Kennedy, and A. Kuzmich, Nature **438**, 833 (2005).
[8] S. Olmschenk, D. N. Matsukevich, P. Maunz, D. Hayes, L.-M. Duan, and C. Monroe, Science **323**, 486 (2009).
[9] B. D. Gerardot, D. Brunner, P. A. Dalgarno, P. Öhberg, S. Seidl, M. Kroner, K. Karrai, N. G. Stoltz, P. M. Petroff, and R. J. Warburton, Nature **451**, 441 (2008).
[10] M. H. Devoret and R. J. Schoelkopf, Science **339**, 1169 (2013).
[11] H. J. Kimble, Nature **453**, 1023 (2008).
[12] S. Tanzilli, W. Tittel, M. Halder, O. Alibart, P. Baldi, N. Gisin, and H. Zbinden, Nature **437**, 116 (2005).
[13] J. Huang and P. Kumar, Phys. Rev. Lett. **68**, 2153 (1992).
[14] P. Kumar, Opt. Lett. **15**, 1476 (1990).
[15] M. Mirhosseini, A. Sipahigil, M. Kalaee, and O. Painter, Nature **588**, 599 (2020).
[16] R. W. Andrews, R. W. Peterson, T. P. Purdy, K. Cicak, R. W. Simmonds, C. A. Regal, and K. W. Lehnert, Nature Physics **10**, 321 (2014).
[17] M. T. Rakher, L. Ma, O. Slattery, X. Tang, and K. Srinivasan, Nature Photonics **4**, 786 (2010).
[18] T. Kitagawa, E. Berg, M. Rudner, and E. Demler, Phys. Rev. B **82**, 235114 (2010).
[19] N. H. Lindner, G. Refael, and V. Galitski, Nature Physics **7**, 490 (2011).
[20] A. C. Potter, T. Morimoto, and A. Vishwanath, Phys. Rev. X **6**, 041001 (2016).
[21] S. Choi, J. Choi, R. Landig, G. Kucsko, H. Zhou, J. Isoya, F. Jelezko, S. Onoda, H. Sumiya, V. Khemani, C. von Keyserlingk, N. Y. Yao, E. Demler, and M. D. Lukin, Nature **543**, 221 (2017).
[22] Y. Peng and G. Refael, Phys. Rev. B **97**, 134303 (2018).
[23] I. Martin, G. Refael, and B. Halperin, Phys. Rev. X **7**, 041008 (2017).
[24] P. J. D. Crowley, I. Martin, and A. Chandran, Phys. Rev. B **99**, 064306 (2019).
[25] D. Malz and A. Smith, "Topological two-dimensional floquet lattice on a single superconducting qubit," (2020), arXiv:2012.01459.
[26] F. Nathan, I. Martin, and G. Refael, Phys. Rev. B **99**, 094311 (2019).

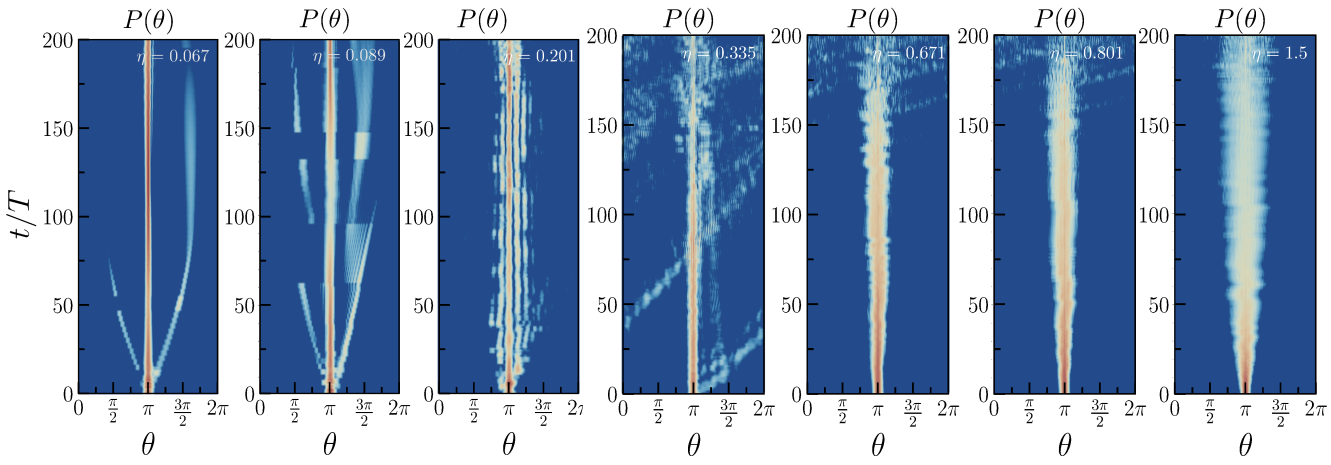

FIG. 14. Time evolution of the phase distribution $P(\theta)$ for parameters ranging between the ultra-weak-drive limit $\eta = 0.067$ up to the strong-drive limit $\eta = 2.236$. We use $B_0 = 1$, $B_m = 8$, $B_d = 8$, $N_{\rm ph} = 20$, and $\omega_1/\omega_2 = 2/3$. In the ultra-weak limit $\eta \ll \omega_i$ (left panel), $P(\theta)$ is described by a central Gaussian peak, suggesting that the phase is preserved during the photon pumping effect. As η is increased further, additional secondary peaks and fluctuations are generated, which suppress quantum coherence. As the system approaches the adiabatic limit $\eta \gg \omega_i$ (right panel), coherence is restored and $P(\theta)$ is well described by a single Gaussian curve. In all depicted cases there is a finite photon pumping effect with $0.6 \leq \bar{n}_F \leq 1$.

[27] E. Abe, H. Wu, A. Ardavan, and J. J. L. Morton, Applied Physics Letters **98**, 251108 (2011).
[28] P. W. Anderson, Phys. Rev. **109**, 1492 (1958).
[29] F. Wegner, Zeitschrift für Physik B Condensed Matter **36**, 209 (1980).
[30] D. J. Thouless, Phys. Rev. B **27**, 6083 (1983).
[31] F. Nathan, G. Refael, M. S. Rudner, and I. Martin, Physical Review Research **2** (2020), 10.1103/physrevresearch.2.043411.
[32] P. Weinberg and M. Bukov, SciPost Phys. **2**, 003 (2017).
[33] L. Privitera, A. Russomanno, R. Citro, and G. E. Santoro, Phys. Rev. Lett. **120**, 106601 (2018).
[34] C. Psaroudaki and G. Refael, "Energy transfer in a random-matrix floquet hamiltonian," (2021), manuscript in prepration.
[35] J. H. Shirley, Phys. Rev. **138**, B979 (1965).
[36] D. Romito, C. Lobo, and A. Recati, The European Physical Journal D **72**, 135 (2018).
[37] D. R. Hofstadter, Phys. Rev. B **14**, 2239 (1976).
[38] F. Evers and A. D. Mirlin, Rev. Mod. Phys. **80**, 1355 (2008).
[39] A. D. Mirlin, Y. V. Fyodorov, F.-M. Dittes, J. Quezada, and T. H. Seligman, Phys. Rev. E **54**, 3221 (1996).
[40] J. Wang and J. Gong, Phys. Rev. Lett. **102**, 244102 (2009).
[41] D. T. Pegg and S. M. Barnett, Phys. Rev. A **39**, 1665 (1989).
[42] D. F. Walls and G. J. Milburn, Quantum optics (Springer, 1995).
[43] M. Tavis and F. W. Cummings, Phys. Rev. **170**, 379 (1968).
[44] H. Huebl, C. W. Zollitsch, J. Lotze, F. Hocke, M. Greifenstein, A. Marx, R. Gross, and S. T. B. Goennenwein, Phys. Rev. Lett. **111**, 127003 (2013).
[45] Y. Tabuchi, S. Ishino, T. Ishikawa, R. Yamazaki, K. Usami, and Y. Nakamura, Phys. Rev. Lett. **113**, 083603 (2014).
[46] X. Zhang, C.-L. Zou, L. Jiang, and H. X. Tang, Phys. Rev. Lett. **113**, 156401 (2014).
[47] H. Maier-Flaig, M. Harder, R. Gross, H. Huebl, and S. T. B. Goennenwein, Phys. Rev. B **94**, 054433 (2016).
[48] N. Kostylev, M. Goryachev, and M. E. Tobar, Applied Physics Letters **108**, 062402 (2016).
[49] Y. Kubo, F. R. Ong, P. Bertet, D. Vion, V. Jacques, D. Zheng, A. Dréau, J.-F. Roch, A. Auffeves, F. Jelezko, J. Wrachtrup, M. F. Barthe, P. Bergonzo, and D. Esteve, Phys. Rev. Lett. **105**, 140502 (2010).
[50] D. I. Schuster, A. P. Sears, E. Ginossar, L. DiCarlo, L. Frunzio, J. J. L. Morton, H. Wu, G. A. D. Briggs, B. B. Buckley, D. D. Awschalom, and R. J. Schoelkopf, Phys. Rev. Lett. **105**, 140501 (2010).
[51] I. Gimeno, W. Kersten, M. C. Pallarés, P. Hermosilla, M. J. Martínez-Pérez, M. D. Jenkins, A. Angerer, C. Sánchez-Azqueta, D. Zueco, J. Majer, A. Lostao, and F. Luis, ACS Nano **14**, 8707 (2020).
[52] S. Körber, L. Privitera, J. C. Budich, and B. Trauzettel, Phys. Rev. Research **2**, 022023 (2020).
[53] J. M. Fink, R. Bianchetti, M. Baur, M. Göppl, L. Steffen, S. Filipp, P. J. Leek, A. Blais, and A. Wallraff, Phys. Rev. Lett. **103**, 083601 (2009).
[54] X. Mi, J. V. Cady, D. M. Zajac, P. W. Deelman, and J. R. Petta, Science **355**, 156 (2017).
[55] X. Mi, M. Benito, S. Putz, D. M. Zajac, J. M. Taylor, G. Burkard, and J. R. Petta, Nature **555**, 599 (2018).
[56] A. J. Landig, J. V. Koski, P. Scarlino, U. C. Mendes, A. Blais, C. Reichl, W. Wegscheider, A. Wallraff, K. Ensslin, and T. Ihn, Nature **560**, 179 (2018).
[57] J. D. Breeze, E. Salvadori, J. Sathian, N. M. Alford, and C. W. M. Kay, npj Quantum Information **3**, 40 (2017).
[58] Z. Fedorova, H. Qiu, S. Linden, and J. Kroha, Nature Communications **11**, 3758 (2020).